Applying the Kelvin probe to biological tissues: Theoretical and computational analyses

Andrew C. Ahn,[1,*,†] Brian J. Gow,[1,†] Ørjan G. Martinsen,[2,3] Min Zhao,[4,5] Alan J. Grodzinsky,[6] and Iain D. Baikie[7]

[1]*Martinos Center for Biomedical Imaging, Massachusetts General Hospital, 149 Thirteenth Street, Charlestown, Massachusetts 02129, USA*
[2]*Department of Physics, University of Oslo, NO-0316 Oslo, Norway*
[3]*Department of Biomedical and Clinical Engineering, Rikshospitalet, Oslo University Hospital, NO-0027 Oslo, Norway*
[4]*Dermatology & Ophthalmology Research Institute for Regenerative Cures, UC Davis School of Medicine,*
2921 Stockton Boulevard, Sacramento, California 95817, USA
[5]*School of Medical Sciences, University of Aberdeen, Aberdeen AB25 2ZD, United Kingdom*
[6]*Center for Biomedical Engineering, Massachusetts Institute of Technology, 77 Massachusetts Avenue, Cambridge,*
Massachusetts 02139, USA
[7]*KP Technology Ltd., Wick KW1 5LE, United Kingdom*

The Kelvin probe measures surface electrical potential without making physical contact with the specimen. It relies on capacitive coupling between an oscillating metal tip that is normal to a specimen's surface. Kelvin probes have been increasingly used to study surface and electrical properties of metals and semiconductors and are capable of detecting material surface potentials with submillivolt resolution at a micrometer spatial scale. Its capability for measuring electrical potential without being confounded by electrode-specimen contact makes extending its use towards biological materials particularly appealing. However, the theoretical basis for applying the Kelvin probe to dielectric or partially conductive materials such as biological tissue has not been evaluated and remains unclear. This study develops the theoretical basis underlying Kelvin probe measurements in five theoretical materials: highly conductive, conductive dielectric with rapid charge relaxation, conductive dielectric with slow charge relaxation, perfect dielectric, and tissue with a bulk serial resistance. These theoretically derived equations are then computationally analyzed using parameters from both theoretical specimens and actual biomaterials—including wet skin, dry skin, cerebrospinal fluid, and tendon. Based on these analyses, a Kelvin probe performs in two distinct ways depending on the charge relaxation rates of the sample: The specimen is treated either as a perfect dielectric or as highly conductive material. Because of their rapid relaxation rate and increased permittivity biomaterials behave similarly to highly conductive materials, such as metal, when evaluated by the Kelvin probe. These results indicate that the Kelvin probe can be readily applied to studying the surface potential of biological tissue.

PACS number(s): 87.15.A−, 87.15.Pc, 87.19.R−, 87.50.C−

I. INTRODUCTION

A Kelvin probe measures a specimen's surface electrical potential without making physical contact and utilizes a vibrating metallic tip placed over a specimen of interest. These two components are connected to form a circuit, as detailed in the next section. The metallic tip and specimen form the two contralateral components of a capacitor and, with a given electrical potential difference, their proximity induces the accumulation of opposing charges on their respective surfaces. The oscillating probe tip alters the capacitance and thus, by extension, the surface charges on both the tip and the specimen. This process generates an oscillating current which is captured and converted to a voltage by the Kelvin probe measurement system to ultimately determine the potential difference between the tip and the specimen [1].

Although the Kelvin probe was first postulated by Sir William Thomson (Lord Kelvin) as early as the 1860s, advances in metallic tip fabrication, motor controllers, microchips, and software engineering have led to its increasing utilization across a broad range of disciplines—including corrosion science [2,3], liquid-air interfaces [4,5], surface adsorption [6], polymer science and engineering [7], and semiconductor studies [8–12], among others. At present, the Kelvin probe is capable of detecting material surface potentials with submillivolt resolution at a micrometer spatial scale. Moreover, the development of an "off-null" detection method (to be discussed later) has greatly enhanced the signal-to-noise ratio and permits the independent reporting of the tip-to-specimen spacing to within 1 μm [13–15].

Because the Kelvin probe measures surface potential without actually touching the specimen, it has substantial advantages over existing potentiometer devices and can conceivably be used to evaluate biological specimens in the *in vivo* setting. It is not limited by variable ion accumulation at the electrode, the effects of contact medium, or the influence of mechanical pressure on the specimen, and thus bypasses the electrode-tissue confounders that plague most, if not all, conventional electrical measurement devices. In addition, the Kelvin probe does not utilize intercalating dyes, strong electrical currents, or ionizing beams that may interfere or possibly harm active physiologic processes. For these reasons, several studies have investigated the use of the Kelvin probe in biological events—specifically, corn shoot growth [1] and human skin wound [16]—and have identified measurable and possibly physiologically meaningful surface potentials. Nevertheless, the theoretical basis for applying the Kelvin

---

*Corresponding author: aahn1@partners.org
†These authors contributed equally to this study and are listed in alphabetic order.
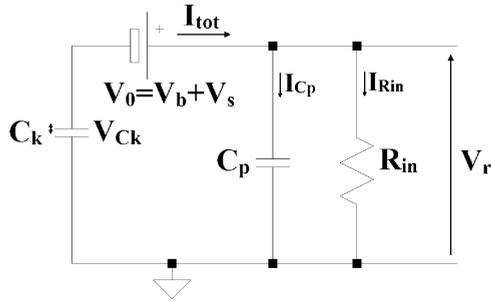
FIG. 1. Circuit diagram for a Kelvin probe testing a specimen where V_0 is equal to the constant intrinsic potential difference between the tip and specimen, V_s, plus an applied dc backing potential, V_b. V_{Ck} is the oscillatory component stemming from the vibrating tip.

probe to biological specimens has not been evaluated and still remains unclear.

Kelvin probes have traditionally been applied to highly conductive materials such as metals because the results are interpretable: The charge carrier is well defined (i.e., electron) and the Kelvin probe-derived surface potential measurements impart information about the substance's work function (i.e., the minimum energy required to liberate an electron from the surface). In biological tissue, however, the charge carriers are typically ionic; the fixed molecular constituents have insulating and often polar properties; and the charge relaxation process is not as instantaneous as it is in metal. In order to understand the factors contributing to the Kelvin probe measurements in biological specimens, this study develops the theoretical basis underlying Kelvin probe measurements in five theoretical materials: highly conductive, conductive dielectric with rapid charge relaxation, conductive dielectric with slow charge relaxation, perfect dielectric, and tissue with a bulk serial resistance. These theoretically derived equations are then computationally analyzed using parameters from both theoretical specimens and actual biomaterials.

II. THE ANALYTICAL MODEL

To fully derive the theoretical equations, two aspects of our analyses must be defined: first, the Kelvin probe electrical

circuit and second, the electrical constitutive and conservative relationships within the theoretical specimen.

A basic circuit diagram of a Kelvin probe is provided in Fig. 1 and is based on prior publications [14] and an available device on the market (SKP 5050, KP Technology Ltd., Wick, UK) but can be generalized to other similar devices. The variable capacitance arising from the oscillating probe tip over a stationary specimen is represented by C_k. The constant intrinsic potential difference between the probe tip and the specimen is symbolized by V_s. This potential difference may be supplemented by an applied dc voltage referred to as V_b, or the backing potential. Shown in Fig. 1, V_0 represents V_s plus the backing potential, V_b: $V_0 = V_s + V_b$. V_{Ck} represents the oscillatory component of the voltage stemming from the vibrating tip. The oscillating capacitance at a given voltage difference, V_0, generates an oscillating current, I_{tot}, which is distributed to the system's input resistance, R_{in}, and parasitic capacitance, C_p. The voltage at the input to the system's current-to-voltage (I-V) converter is noted as V_r.

The backing potential V_b can be manipulated by the user and is traditionally varied until the current flowing through the circuit—and thus V_r—is zero. Because this occurs when $V_b = -V_s$ this approach is often used to derive the intrinsic potential difference between the probe tip and the specimen. However, the presence of external electrical fields and circuit noise at the zero current level present significant barriers for the exact determination of this value, and for this reason, an off-null approach is often used. This will be further described in a subsequent section (Sec. III B 1).

The constitutive and conservative relationships within the theoretical and biomaterial specimens will follow the model illustrated in Fig. 2. The mean distance between the probe tip and specimen is given as d_0 and the amplitude of the tip oscillation given by d_a. In highly conductive substances such as metal, the electrical field is effectively neutralized at the very superficial layers (approximately a few angstroms) due to the mobile charges within the specimen. This results in a single capacitor between the Kelvin probe tip and specimen, and, as depicted in Fig. 2(a), eliminates any contributing field effects from the material bulk below the surface. The potential drop across this capacitor is represented by V_c. This model will be used for the highly conductive material case.
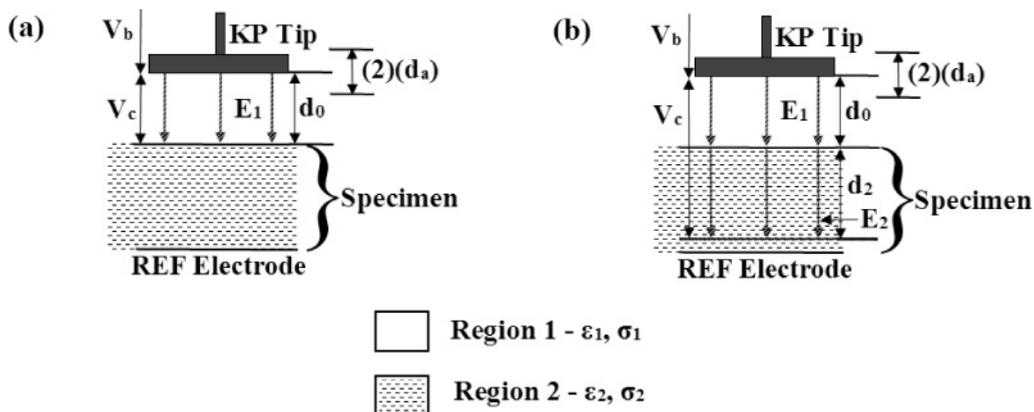
FIG. 2. In both figures the region is indicated by the subscript number. (a) Diagram showing the electrical field, E, from the Kelvin probe being neutralized at a very superficial layer within the specimen. (b) Diagram showing the electrical field, E, from the Kelvin probe penetrating the specimen prior to being neutralized.
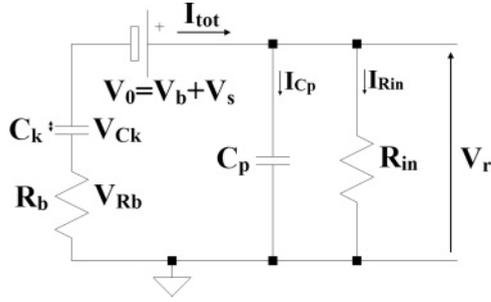
FIG. 3. Circuit diagram for a Kelvin probe testing a specimen which has a bulk resistance, R_b.

Most biomaterials, on the contrary, are neither pure conductors nor perfect dielectrics. By definition, dielectric materials allow electrical fields to penetrate and thereby lend to the contributions of bulk conductivity and permittivity to the overall charge aggregation on the probe tip. Figure 2(b) illustrates this process and demarcates the properties associated with each region. In the perfect dielectric case, the conductivity in Region 2, σ_2, is zero and is conceptually represented by two capacitors in series: one across air and a second across the dielectric specimen. In the conductive dielectric cases, both ε_2, the permittivity in Region 2, and σ_2 have nonzero values and are associated with charge relaxation rates that are either much slower or much faster than the tip oscillation rates. These divergent cases will be treated separately. In Fig. 2(b), V_c represents the potential drop across both capacitors while the depth of the specimen capacitor is represented by d_2. This depth can vary greatly depending on the material properties of the specimen.

The final theoretical case, resistive bulk, involves a resistive component within the bulk tissue and specifically evaluates the effects of the bulk-traversing electrical currents on the Kelvin probe potential measurements. As shown in Fig. 3, a resistor is added in series with the tip-to-specimen capacitor.

For each of these theoretical cases, the governing equations and mathematical derivation of V_r (during tip oscillations) are detailed separately in the following section. In situations where the solutions were too complex for manual derivations, a symbolic computation program, MAPLE v.15 (Maplesoft, Waterloo, Ontario, Canada), was used. This software was also employed to numerically compute the anticipated V_r measurements for our representative theoretical and biomaterial specimens.

III. MATERIAL FORMULATIONS

A. Tip electric field

To derive the result for V_r for each theoretical case we must understand the electrical field, E_1, at the tip of the Kelvin probe. To establish this solution, the conductive current within the specimen must be elaborated and used to determine E_1, the electrical field between tip and specimen as a function of the Region 1 and 2 properties as depicted in Fig. 2(b). The boundary condition at the interface between Regions 1 and 2 associated with the law of charge conservation yields the following formula:

$$\hat{n} \bullet (J_2 - J_1) + \nabla_\Sigma \bullet K = -\frac{\partial \sigma_s}{\partial t}, \quad (3.1)$$

where J is the current density in the indicated region. The surface charge density is given by σ_s. The presence of a surface current at the interface is accounted for by K. The $\nabla_\Sigma \bullet K$ term denotes the divergence of K in the plane of the surface [17]. Surface currents can arise from a parallel (to the surface) component of the electrical field and can be represented by a stray capacitive effect. The stray capacitive effect on the Kelvin probe measurement will not be directly considered here as it has been evaluated previously [14]. In the analysis performed here we assume the placement of the reference electrode is such that the electrical field perpendicular to the specimen greatly exceeds the tangential component of the electrical field. This implies that the surface current term in Eq. (3.1) is negligible, so it can be simplified to

$$\hat{n} \bullet (J_2 - J_1) = -\frac{\partial \sigma_s}{\partial t}. \quad (3.2)$$

However, if the sample area under the tip is closely proximate to the reference electrode and if the surface conductivity between the two areas is large, this simplification cannot be made because the surface current density would not be negligible. The interfacial (boundary) condition associated with Gauss' law states that

$$\sigma_s = \hat{n} \bullet (\varepsilon_2 E_2 - \varepsilon_1 E_1), \quad (3.3)$$

where E is the electrical field in the indicated region. The permittivity for a given region is indicated by ε. The current density in each region is given by

$$J_2 = \sigma_2 E_2, \quad (3.4)$$

$$J_1 = \sigma_1 E_1, \quad (3.5)$$

where the conductivity in an indicated region is given by σ. Region 1 is typically air and has a nonzero capacitive current component but an Ohmic (conduction) component equal to zero. Given this constraint we combine Eqs. (3.2)–(3.5) resulting in

$$\hat{n} \bullet \sigma_2 E_2 = -\frac{\partial [\hat{n} \bullet (\varepsilon_2 E_2 - \varepsilon_1 E_1)]}{\partial t}. \quad (3.6)$$

Since fringing fields are assumed negligible, from here forward, the electrical field variables, E_1 and E_2, will represent the normal components of the electrical fields and will thus be given as scalars. The contact potential, V_c, is given by

$$d_1(t) E_1(t) + d_2 E_2 = V_c, \quad (3.7)$$

where $d_1(t) = d_0 + d_a \sin(\omega t)$. The tip oscillation angular frequency is given by ω. Combining the two latter equations [Eqs. (3.6) and (3.7)] and solving for $E_1(t)$ reveals that

$$E_1(t) = \frac{V_c}{d_1(t)} + V_c \left[\frac{\varepsilon_2}{\varepsilon_2 d_1(t) + \varepsilon_1 d_2} - \frac{1}{d_1(t)} \right] e^{-t/\tau}. \quad (3.8)$$

The equation for τ is given by

$$\tau = \frac{(\varepsilon_1 d_2 + \varepsilon_2 d_0)}{(\sigma_2 d_0)}. \quad (3.9)$$

The first term for $E_1(t)$ is the steady state solution while the second term is the transient one. The time constant, τ, is determined by the conductivity of Region 2, along with the permittivity and depth of both regions. It represents the charge

relaxation time for the system after the external electrical field is altered. The equation for E_1 allows for determination of V_r for a variety of biomaterials with different charge relaxation characteristics. In the following sections we consider such solutions for the theoretical cases of interest.

B. Basic circuit material formulations

The basic circuit shown in Fig. 1 serves as the basis for the derivation of the highly conductive, conductive dielectric with rapid relaxation, conductive dielectric with slow relaxation, and perfect dielectric cases presented in this section.

The current generated by the Kelvin probe tip oscillation is distributed across the circuit:

$$\frac{dq}{dt} = I_{\text{tot}} = I_{Cp} + I_{\text{Rin}} = C_p \frac{dV_r}{dt} + \frac{V_r}{R_{\text{in}}}, \quad (3.10)$$

where I_{Cp} is the current through C_p and I_{Rin} is the current through R_{in} as shown in Fig. 1.

From Kirchoff's second law, the following voltage relationship holds:

$$V_{Ck} + V_0 + V_r = 0, \quad (3.11)$$

which can subsequently be rearranged to yield the charge at the probe tip:

$$q = -C_k (V_0 + V_r). \quad (3.12)$$

Taking the derivative of this equation and setting it equal to Eq. (3.10) yields

$$\frac{dV_r}{dt} + \left[\frac{1}{R_{\text{in}}(C_p + C_k)} + \frac{1}{(C_p + C_k)} \frac{dC_k}{dt} \right] V_r$$
$$= -\frac{1}{(C_p + C_k)} \frac{dC_k}{dt} V_0. \quad (3.13)$$

Taking $C_p \gg C_k$ and $1/R_{\text{in}} \gg dC_k/dt$ this equation simplifies to

$$\frac{dV_r}{dt} + \frac{1}{R_{\text{in}}C_p} V_r = -\frac{1}{C_p} \frac{dC_k}{dt} V_0. \quad (3.14)$$

This differential equation can be used to obtain the $V_r(t)$ solution for a particular material that follows the circuit arrangement depicted in Fig. 1.

1. Highly conductive material

As stated previously, Kelvin probes have been extensively used for highly conductive materials such as metals. Here, we revisit the theoretical solution for V_r in such materials as previously described by Baikie et al. [14].

The relative importance of the transient term in Eq. (3.8) depends on the time scale by which the electrical fields are being modified. With respect to the Kelvin probe, the time variation in electrical field magnitudes arises from the oscillating specimen-to-tip distance: Assuming a fixed tip-to-specimen potential difference, the electrical field amplitude increases as the tip-to-specimen distance decreases and conversely decreases as the distance increases. For a voice-coil actuator Kelvin probe the oscillation period is typically between 10 and 30 ms. If the tip oscillating period, t_1, is substantially longer than the charge relaxation time ($\tau \ll t_1$)—as it is for a highly conductive material with very rapid charge relaxation—then

the transient exponent $\exp(-t_1/\tau)$ rapidly approaches zero during each period of the sinusoid. This leaves the following equation for E_1:

$$E_1(t) = \frac{V_c(t)}{d_1(t)}. \quad (3.15)$$

The capacitance, C_k, is given by

$$C_k = \frac{q}{V_c} = \frac{\sigma_s A}{V_c} = \frac{\varepsilon_1 E_1 A}{V_c}. \quad (3.16)$$

The area of the capacitor plates, A, can be taken as $(\pi)(r^2)$, where r is the radius of the Kelvin probe tip. Plugging $E_1(t)$ for this case into C_k simplifies it to the familiar form

$$C_k = \frac{\varepsilon_1 A}{d_1(t)}. \quad (3.17)$$

Solving the differential equation for $V_r(t)$ given in Eq. (3.14), while using the C_k provided above and making the assumption that $d_0 \gg d_a$, it is observed that

$$V_r(t) = -\frac{\omega b}{a^2 + \omega^2} e^{-at} + \frac{b}{\sqrt{a^2 + \omega^2}} \sin(\omega t + \theta), \quad (3.18)$$

where

$$a = \frac{1}{R_{\text{in}}C_p}, \quad b = \frac{V_0 \omega \varepsilon_1 d_a A}{C_p d_0^2}, \quad \theta = \tan^{-1}\left(-\frac{\omega}{a}\right).$$

The first term in Eq. (3.18) is the transient while the second term represents the steady state solution. The steady state solution can be written as

$$V_{ss}(t) = \frac{K_M}{d_0^2} (V_b + V_s) \sin(\omega t + \theta), \quad (3.19)$$

where

$$K_M = \frac{\omega \varepsilon_1 d_a A}{C_p \sqrt{\frac{1}{R_{\text{in}}^2 C_p^2} + \omega^2}}.$$

The peak-to-peak voltage is

$$V_{ptp} = \frac{2K_M}{d_0^2} (V_b + V_s). \quad (3.20)$$

The Kelvin probe primarily utilizes this peak-to-peak value to calculate V_s, the surface potential difference between the tip and the specimen. As shown in Fig. 4, by varying V_b and simultaneously recording V_{ptp}, a linear V_{ptp} versus V_b plot is produced. The x intercept occurs when V_b is equal to $-V_s$. A change in V_s will cause the line to shift either to the right or to the left. On the other hand, a change in d_0—the mean distance between the tip and specimen—will change the slope of the line without affecting its x-axis intercept. The slope of the V_{ptp} versus V_b line is termed GD for gradient and can be used to maintain a constant tip-to-specimen distance since GD is inversely proportional to d_0 squared:

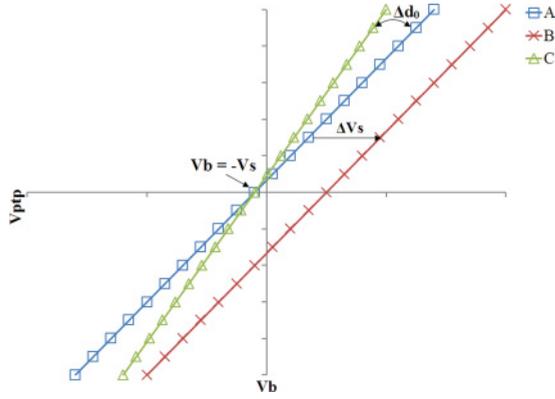$$GD \alpha \frac{1}{d_0^2}. \quad (3.21)$$

FIG. 4. (Color online) V_{ptp} versus V_b plot showing its relationship to ΔV_s and Δd_0. A change in specimen surface potential, V_s, shifts the result horizontally along the V_b axis, as seen between lines A and B. Changing the tip-to-specimen distance changes the slope as seen between lines A and C.

Given these relationships, an off-null method can be used to determine V_s by using two V_b levels in the linear regime: $V_b \gg V_s$ and $V_b \ll V_s$, as described by Baikie *et al.* [1]. A linear projection between the two points can help extrapolate the x intercept and thus derive V_s. This off-null approach minimizes the noise frequently associated with self-nulling systems where external and internal noises can significantly confound the determination of the zero current point. The off-null approach may also be used to calculate GD and can be incorporated into a "tracking" software algorithm to maintain a constant tip-to-specimen distance [1]. With tracking enabled, adjustments of the tip-to-specimen distance are made by the system's stepper motors prior to making a V_s measurement. This can be particularly helpful when scanning across an uneven surface or testing a moving specimen. Holding the tip-to-specimen distance constant assures minimal variation in d_0 and thus C_k.

2. Conductive dielectric with rapid relaxation

Biomaterials typically have free and bound charges. For this reason, materials with nonzero conductivity and permittivity values are considered here. While the mechanism of charge relaxation within a dielectric is very different than that in a metal its effect on the transient term in Eq. (3.8) is similar. For this rapid relaxation case we once again assume that any charge relaxation occurs at a time scale much shorter than the Kelvin probe oscillation period. This yields the condition $\tau \ll t_1$. Therefore the electrical field at the probe tip can be simplified to (3.15). It then follows that the solutions for C_k, V_r, V_{ss}, and V_{ptp} for this case are the same as in the highly conductive material case, shown in Eqs. (3.16), (3.18), (3.19), and (3.20), respectively.

Despite the presence of a polarizable molecular substrate, the high conductivity of the substrate and the associated short charge relaxation time results in close to zero electric field in Region 2. Thus, polarization effects in Region 2 are negligible, accounting for a rapid response to changes in the external electrical field similar to that of highly conductive materials such as metal. Conductivity is a general term referring to any type of mobile charge and thus may refer to ionic conductivity

as well as electrical conductivity. Importantly, as noted in the formula for the time constant, Eq. (3.9), d_0 and d_2 also play a contributory role and should be factored in when determining whether a dielectric is categorized as having "rapid relaxation."

3. Conductive dielectric with slow relaxation

Next, we consider a conductive dielectric with slow relaxation, $\tau \gg t_1$. In this case, the material response to the electrical field is much slower than the rate at which the electrical field is changed due to the Kelvin probe tip oscillations. Consequently, the transient term for $E_1(t)$ in Eq. (3.8) is no longer negligible and must be incorporated into the $V_r(t)$ calculations. Substituting $E_1(t)$ into Eq. (3.16), the composite capacitance is shown here:

$$C_k = \varepsilon_1 A \left\{ \frac{1}{d_1(t)} + \left[\frac{\varepsilon_2}{\varepsilon_2 d_1(t) + \varepsilon_1 d_2} - \frac{1}{d_1(t)} \right] e^{-t/\tau} \right\}.$$

(3.22)

To solve for $V_r(t)$, C_k is substituted into Eq. (3.14). It is assumed that $d_0 \gg d_a$ and since $\tau \gg t_1$, the exponential term $\exp(-t/\tau)$ is assumed to be constant during the actual symbolic solution of the differential equation. From the perspective of the specimen, this assumption suggests that no meaningful response in charge relaxation is observed within the span of the Kelvin probe measurement period. The complete symbolic solution for $V_r(t)$ is

$$V_r(t) = -\frac{\varepsilon_1 A R_{\text{in}} (V_{N1} + V_{N2} + V_{N3} + V_{N4})}{(d_0^2 \tau)(\varepsilon_2 d_0 + \varepsilon_1 d_2)^2 (1 + \omega^2 R_{\text{in}}^2 C_p^2)} (V_b + V_s),$$

(3.23)

where

$$V_{N1} = e^{-t/R_{\text{in}}C_p} e^{-t/\tau} \left[\left(-\varepsilon_1 \varepsilon_2 d_2 d_0^2 - \varepsilon_1^2 d_2^2 d_0 \right) \left(1 + \omega^2 R_{\text{in}}^2 C_p^2 \right) \right.$$
$$\left. + \left(d_a \omega^2 \tau R_{\text{in}} C_p \right) \left(-2\varepsilon_2 \varepsilon_1 d_0 d_2 - \varepsilon_1^2 d_2^2 \right) \right],$$

$$V_{N2} = e^{-t/R_{\text{in}}C_p} [d_a \omega^2 \tau R_{\text{in}} C_p (\varepsilon_2 d_0 + \varepsilon_1 d_2)^2],$$

$$V_{N3} = e^{-t/\tau} \left\{ \left(\varepsilon_1 \varepsilon_2 d_2 d_0^2 + \varepsilon_1^2 d_2^2 d_0 \right) \left(1 + \omega^2 R_{\text{in}}^2 C_p^2 \right) \right.$$
$$+ \left(d_a \tau \omega \right) \left(\varepsilon_1^2 d_2^2 + 2\varepsilon_1 \varepsilon_2 d_0 d_2 \right) [\omega R_{\text{in}} C_p \cos(\omega t)$$
$$\left. - \sin(\omega t)] \right\},$$

$$V_{N4} = (d_a \omega \tau)(\varepsilon_2 d_0 + \varepsilon_1 d_2)^2 [\sin(\omega t) - \omega R_{\text{in}} C_p \cos(\omega t)].$$

Taking $\exp(-t/\tau)$ to be equal to 1 and simplifying, it can be shown that the steady state solution is

$$V_{ss} = K_S(V_b + V_s) \sin(\omega t + \theta) + V_{dc}, \quad (3.24)$$

where

$$K_S = \frac{\omega \varepsilon_1 \varepsilon_2^2 d_a A}{(\varepsilon_2 d_0 + \varepsilon_1 d_2)^2 C_p \sqrt{\frac{1}{R_{\text{in}}^2 C_p^2} + \omega^2}}.$$

θ is the same as in Eq. (3.18) and V_{dc} is a dc voltage associated with the solution. Table I provides the equation for V_{dc}. Generally, V_{dc} is small relative to the oscillatory component and does not affect the V_{ptp} measure of the Kelvin probe which is given by

$$V_{ptp} = 2K_S(V_b + V_s). \quad (3.25)$$

TABLE I. Theoretical equation summary.

Parameter	Highly conductive	Rapid relaxation	Slow relaxation	Perfect dielectric	Resistive bulk
Dc offset (V_r)	0	0	SNZ1	0	0
Phase (V_r)	$\tan^{-1}(-R_{in}C_p\omega)$	$\tan^{-1}(-R_{in}C_p\omega)$	$\tan^{-1}(-R_{in}C_p\omega)$	$\tan^{-1}(-R_{in}C_p\omega)$	SN1
V_{ptp}	(3.20)	(3.20)	(3.25)	(3.32)	(3.40)
GD	$\dfrac{2\omega\varepsilon_1 d_a A}{d_0^2 C_p\sqrt{\frac{1}{R_{in}^2 C_p^2}+\omega^2}}$	$\dfrac{2\omega\varepsilon_1 d_a A}{d_0^2 C_p\sqrt{\frac{1}{R_{in}^2 C_p^2}+\omega^2}}$	$\dfrac{2\omega\varepsilon_1\varepsilon_2^2 d_a A}{(\varepsilon_2 d_0+\varepsilon_1 d_2)^2 C_p\sqrt{\frac{1}{R_{in}^2 C_p^2}+\omega^2}}$	$\dfrac{2\omega\varepsilon_1\varepsilon_2^2 d_a A}{(\varepsilon_2 d_0+\varepsilon_1 d_2)^2 C_p\sqrt{\frac{1}{R_{in}^2 C_p^2}+\omega^2}}$	SN2
GD versus d_0	$\sim\dfrac{1}{d_0^2}$	$\sim\dfrac{1}{d_0^2}$	$\sim\dfrac{1}{d_0^2+d_0}$	$\sim\dfrac{1}{d_0^2+d_0}$	$\sim\dfrac{1}{d_0^2+d_0}$

Designator	Equation
SNZ1	$\dfrac{\varepsilon_1 A R_{in}\left(\varepsilon_1^2 d_2^2 d_0+\varepsilon_1\varepsilon_2 d_0^2 d_2+\varepsilon_1^2 d_2^2 d_0\omega^2 R_{in}^2 C_p^2+\varepsilon_1\varepsilon_2 d_0^2 d_2\omega^2 R_{in}^2 C_p^2\right)}{(d_0^2\tau)(\varepsilon_2 d_0+\varepsilon_1 d_2)^2(1+\omega^2 R_{in}^2 C_p^2)}(V_b+V_s)$
SN1	$\tan^{-1}\left(\dfrac{R_{in}d_2\varepsilon_1 C_p\omega+R_{in}d_0\varepsilon_2 C_p\omega}{R_{in}R_b\varepsilon_1\varepsilon_2 AC_p\omega^2-d_2\varepsilon_1-d_0\varepsilon_2}\right)$
SN2	$\dfrac{2R_{in}\varepsilon_2^2\varepsilon_1 d_a A\omega}{(d_0\varepsilon_2+d_2\varepsilon_1)\sqrt{(R_{in}R_b\varepsilon_1\varepsilon_2 AC_p\omega^2-d_2\varepsilon_1-d_0\varepsilon_2)^2+(R_{in}C_p\omega)(d_2\varepsilon_1+d_0\varepsilon_2)^2}}$

The specimen permittivity ε_2 and the effective penetration depth, d_2, are influential in K_S. The relationship between GD and d_0 is more complicated than that of the highly conductive and rapid relaxation cases. A change in d_0 will now cause the slope to change with

$$GD\alpha\frac{1}{d_0^2+d_0}, \qquad (3.26)$$

as opposed to the $1/d_0^2$ relationship in a metal. For cases where $\varepsilon_2 d_0\gg\varepsilon_1 d_2$ the behavior will be similar to that in a highly conductive material since the slope will be proportional to $1/d_0^2$.

Also for this case where $\varepsilon_2 d_0\gg\varepsilon_1 d_2$, $(\varepsilon_2 d_0+\varepsilon_1 d_2)^2$ will be dominated by $\varepsilon_2^2 d_0^2$. Due to the ε_2^2 term in the numerator of K_S, these will cancel, implying that the permittivity of Region 2 does not significantly affect the result in this scenario.

The solution in Eq. (3.23) highlights the importance of the relative relationship between the Kelvin probe capture point and the relaxation time. The off-null approach requires V_b to be switched between two values. If V_b is held constant for a prolonged period of time prior to switching, Eq. (3.23) is reduced to just the V_{N4} term as $t\to\infty$, and the specimen functions similarly to a highly conductive material. On the other hand, immediate switching relative to relaxation time, as it is assumed here ($t<100*\tau$), would generate a much different response.

4. Perfect dielectric

Unlike highly conductive materials and conductive dielectrics which have free charges available to neutralize external electrical fields, perfect dielectrics (i.e., perfect insulators) theoretically have no free charges [18]. The response to an electrical field in a perfect dielectric is confined to the rotation of bound charges within the specimen. The charges are not free to migrate to the superficial layers of the specimen. The localized reorientation of these charges serves to counter the external electrical field. A perfect dielectric being tested by

a Kelvin probe is represented in Fig. 2(b) with specimen conductivity approaching zero. The depth of the capacitor would not vary significantly with time due to the absence of mobile charges. By allowing the specimen conductivity to approach zero, the relaxation time, τ, will be large and the exponent in (3.8), $\exp(-t/\tau)$, approximates to 1. This eliminates the $V_c/d_1(t)$ terms and yields the following $E_1(t)$ relationship:

$$E_1(t)=\frac{V_c\varepsilon_2}{\varepsilon_2 d_1(t)+\varepsilon_1 d_2}. \qquad (3.27)$$

Combining this with Eq. (3.16) we observe that the capacitance in this case is simply represented by two ideal capacitors below the tip:

$$C_k=\left[\frac{d_1(t)}{\varepsilon_1 A}+\frac{d_2}{\varepsilon_2 A}\right]^{-1}. \qquad (3.28)$$

Taking the derivative of C_k with respect to time yields

$$\frac{dC_k}{dt}=\frac{d_a\omega\sin(\omega t)}{\varepsilon_1 A\left[\frac{d_1(t)}{\varepsilon_1 A}+\frac{d_2}{\varepsilon_2 A}\right]^2}. \qquad (3.29)$$

Solving Eq. (3.14) for this condition yields

$$V_r(t)=-\frac{\omega b}{a^2+\omega^2}e^{-at}+\frac{b}{\sqrt{a^2+\omega^2}}\sin(\omega t+\theta), \quad (3.30)$$

where

$$a=\frac{1}{R_{in}Cp},\quad b=\frac{V_0\omega d_a A\varepsilon_1\varepsilon_2^2}{C_p(\varepsilon_2 d_0+\varepsilon_1 d_2)^2},\quad \theta=\tan^{-1}\left(-\frac{\omega}{a}\right).$$

The steady state solution is then

$$V_{ss}(t)=K_P(V_b+V_s)\sin(\omega t+\theta), \qquad (3.31)$$

where

$$K_P=\frac{\omega\varepsilon_1\varepsilon_2^2 d_a A}{(\varepsilon_2 d_0+\varepsilon_1 d_2)^2 C_p\sqrt{\frac{1}{R_{in}^2 C_p^2}+\omega^2}}.$$

This results in a peak-to-peak voltage of

$$V_{ptp} = 2K_P(V_b + V_s). \tag{3.32}$$

This solution is identical to Eq. (3.25) for a conductive dielectric with slow relaxation, which follows from taking the exponent in (3.8) equal to 1.

C. Resistive bulk formulation

A material which exhibits resistance between the effective penetration depth within the specimen to the reference electrode is considered here. The circuit diagram for this case is shown in Fig. 3.

Applying conservation of potential to this circuit, the potential drop across R_b is noted to be

$$V_{Rb} = I_{\text{tot}} R_b = \frac{dq}{dt} R_b. \tag{3.33}$$

The potential drops across the circuit elements are, therefore,

$$V_{Rb} + V_{Ck} + V_0 + V_r = \frac{dq}{dt} R_b + \frac{q}{C_k} + V_0 + V_r = 0. \tag{3.34}$$

Rearranging this equation gives

$$\frac{dq}{dt} R_b C_k + q = -C_k (V_0 + V_r). \tag{3.35}$$

Taking the derivative of this equation with respect to time yields

$$\frac{d^2q}{dt^2} R_b C_k + \frac{dq}{dt} \frac{dC_k}{dt} R_b + \frac{dq}{dt}$$
$$= -C_k \frac{dV_r}{dt} - \frac{dC_k}{dt} (V_0 + V_r). \tag{3.36}$$

Taking the derivative of Eq. (3.10) with respect to time yields

$$\frac{d^2q}{dt^2} = C_p \frac{d^2V_r}{dt^2} + \frac{1}{R_{\text{in}}} \frac{dV_r}{dt}. \tag{3.37}$$

We get the following differential equation for V_r by combining the above equations:

$$\frac{d^2V_r}{dt^2} + \frac{dV_r}{dt} \frac{1}{R_b C_k} + V_r \frac{1}{R_b R_{\text{in}} C_p C_k}$$
$$= -\frac{dC_k}{dt} \frac{1}{R_b C_p C_k} (V_0 + V_r), \tag{3.38}$$

assuming $\quad C_p \gg C_k, \quad C_p \gg \dfrac{C_k R_b}{R_{\text{in}}}, \quad \dfrac{1}{R_{\text{in}}} \gg \dfrac{dC_k}{dt},$

$$C_p \gg R_b C_p \frac{dC_k}{dt}, \quad \text{and} \quad \frac{1}{R_{\text{in}}} \gg \frac{R_b}{R_{\text{in}}} \frac{dC_k}{dt}.$$

For the complete solution of $V_r(t)$ see Appendix A [Eq. (A1)].

The steady state solution is

$$V_{ss} = 2K_B (V_b + V_s) \sin(\omega t + \theta), \tag{3.39}$$

where

$$K_B = \frac{R_{\text{in}} \varepsilon_2^2 \varepsilon_1 d_a A \omega}{(d_0 \varepsilon_2 + d_2 \varepsilon_1) \sqrt{(q^2 + v^2)}},$$
$$q = R_{\text{in}} R_b \varepsilon_1 \varepsilon_2 A C_p \omega^2 - d_2 \varepsilon_1 - d_0 \varepsilon_2,$$
$$v = R_{\text{in}} d_2 \varepsilon_1 C_p \omega + R_{\text{in}} d_0 \varepsilon_2 C_p \omega,$$
$$\theta = \tan^{-1} \left(\frac{v}{q} \right).$$

The peak-to-peak voltage is then given by

$$V_{ptp} = 2K_B (V_b + V_s). \tag{3.40}$$

The solution is complicated and filled with multiple terms. In highly conductive materials such as metal, the resistance is negligible between the effective penetration depth to the reference electrode. This may not necessarily be true for all materials and could potentially lead to misinterpretation of the actual Kelvin probe measurement.

D. Equation summary

Table I summarizes the mathematical derivations of relevant Kelvin probe variables for all of the theoretical material cases. The listed parameters include the dc offset of V_r, the phase angle between V_r and the tip oscillation, the value for GD, and the proportional relationship between GD and d_0.

IV. NUMERICAL CALCULATIONS AND DISCUSSION

A. Setup parameters

Using the formulas derived in the previous section, a computational approach was taken to acquire results typically provided by the Kelvin probe device. Table II outlines the general parameters used for these calculations. Generally, the Kelvin probe tip is placed as close as possible to the specimen to maximize the signal voltage and minimize external noise effects. As indicated in Table II, this distance, d_0, will be assumed to be 1 mm. The standard maximum V_s capture rate is approximately 20 Hz and includes two V_{ptp} captures at different V_b levels. Although options for reducing the V_s capture rate are available (e.g., adding digital-to-analog-converter delays or averaging across multiple V_{ptp} at a given V_b), they will not be considered here. The I-V converter feedback resistor, R_f, and

TABLE II. General parameters.

Description	Designator	Value
Mean tip-to-specimen distance	d_0	1 mm
Tip diameter	—	2 mm
Tip oscillation amplitude	d_a	70 μm
Tip oscillation frequency	ω	$(2\pi)(100)$ rad/s
Tip backing potential	V_b	7 V
Specimen surface potential	V_s	0.5 V
Surface potential capture rate	—	20 Hz
I-V input resistance	R_{in}	20 Ω
I-V input capacitance	C_p	100 pF
I-V feedback resistance	R_f	1×10^7 Ω
Preamplifier gain	G	-1×10^3

TABLE III. Case parameters.

A. Theoretical cases	ε_{r2}	d_2 (m)	τ (s)	R_b (Ω)	
Metal (highly conductive)	—	—	0	0	
Rapid relaxation	—	—	0	0	
Slow relaxation A	1000	1	$(100)(t_1)$	0	
Slow relaxation B	100 000	1	$(100)(t_1)$	0	
Perfect dielectric	1	1	—	0	
Resistive bulk	1	1	—	100	
B. Biological cases	ε_{r2}	σ (S/m)	Calculated d_2 (m)	Assumed d_2 (m)	τ (s)
Cerebrospinal fluid	109	2	35.6	1	4.9×10^{-9}
Tendon	11 857 000	0.305	101	1	3.4×10^{-4}
Wet skin	45298	0.000461	3048	1	8.9×10^{-4}
Dry skin	1135	0.0002	3614	1	9.5×10^{-5}

gain, G, of the preamplifier stage in the Kelvin probe serve to amplify the signal [1]. They are not shown in Figs. 1 or 3, the simplified versions of the Kelvin probe circuits.

Table III A and III B outline the parameters used for the individual theoretical and biological cases. The theoretical parameter values were chosen to highlight the contrasting conditions and cases discussed in the prior section. For example, for the conductive dielectric material with slow relaxation, τ is taken to be 100 times t_1. This creates the extreme condition where the relaxation is slow and allows for the transient exponential term in Eq. (3.22) to be treated as unity. The biological parameter values were taken from published literature [19,20]. The relaxation times were calculated using the formula for τ, as detailed in Eq. (3.9). The depth of the specimen capacitor, d_2, was calculated based on the formula for skin-penetration depth in a lossy conductor:

$$\delta = \frac{1}{\omega\sqrt{\left(\frac{\mu\varepsilon_2}{2}\left\{\sqrt{\left[1+\left(\frac{\sigma}{\omega\varepsilon_2}\right)^2\right]}-1\right\}\right)}}, \quad (4.1)$$

where μ is the permeability of the material and σ the conductivity. Because biological materials are generally nonmagnetic, the permeability can be taken as μ_0, the permeability of free space. As seen in the Table III B, the calculated skin depth is greater than 1 m for all of the biological materials considered. Unless otherwise noted, d_2 is taken to be 1 m. Although the distance between the Kelvin probe tip and the reference electrode is unlikely to be greater than 1 m in most biological specimens, a larger d_2 would highlight the contrasting behaviors of the various biomaterials. The effects of varying d_2 will be discussed further.

B. Theoretical cases

Figures 5(a) and 5(b) provide plots of V_{ss} for the formulations outlined in Sec. III. Unless otherwise noted the highly conductive material will be taken to be a metal. As seen in Fig. 5(a), the V_{ss} solutions for the metal, rapid relaxation and slow relaxation B cases are nearly identical. Closer inspection of the actual numerical data reveals that the slow relaxation B case is associated with minor reductions in peak-to-peak V_{ss} amplitudes. As described in Sec. III B 2, the steady state solution for the rapid relaxation condition reduces to the

metal solution, explaining why the two results are identical. In contrast, the slow relaxation A case yields a substantially smaller V_r amplitude, which can be traced to the following coefficient in the V_{ss} equation (3.24):

$$\frac{\varepsilon_1\varepsilon_2^2}{(\varepsilon_2 d_0 + \varepsilon_1 d_2)^2}. \quad (4.2)$$

Because slow relaxation B has a substantially larger ε_2, the relationship $\varepsilon_2 d_0 \gg \varepsilon_1 d_2$ holds true and the ε_2^2 terms in the numerator and denominator are canceled. Under this condition, the specimen permittivity has little to no effect on the Kelvin probe measurements, and the measures are nearly identical to that of metal. On the other hand, for slow relaxation A, the relationship $\varepsilon_2 d_0 = \varepsilon_1 d_2$ is true and contributes to a fourfold reduction in V_{ss} amplitude. In this regime, changes in ε_2 will affect V_{ss} and generally contribute to smaller V_{ss} amplitudes. Importantly, although an increased ε_2 will generally augment V_{ss} amplitudes, this rule remains valid only once steady state is reached and charge relaxation is effectively complete. The increased ε_2 has the additional effect of substantially increasing the relaxation rate in Eq. (3.9) and thereby effectively reducing the voltage amplitudes in the early stages of relaxation as shown in Eq. (3.23).

In the resistive bulk example, a perfect dielectric specimen is used as its basic component. As shown in Fig. 5(b) the Kelvin probe voltage amplitude observed in a perfect dielectric specimen, with or without a resistive bulk, is substantially decreased when compared to the amplitudes observed for the cases depicted in Fig. 5(a). By having the dielectric specimen possess a dielectric constant equivalent to that of air ($\varepsilon_1 = \varepsilon_2$) and having $d_2 = 1$ m, this hypothetical example presents a situation where the Kelvin probe is effectively measuring a sample nearly 1 m away. Conceptually this makes sense because the dominant term in the denominator of Eq. (4.2) is $\varepsilon_1^2 d_2^2$ in a perfect dielectric specimen. This is not necessarily the situation in the other cases analyzed here. Because the amplitude of V_r is proportional to ε_1/d_0^2 in a metal and $\varepsilon_2^2/(\varepsilon_1 d_2^2)$ in a pure dielectric, the V_r amplitude is six orders of magnitude smaller in the pure dielectric case with the values used here. With a significantly larger ε_2 or smaller d_2, this observed attenuation in amplitude will not be seen. Of note, the added resistance to the bulk has essentially no effect on the V_r amplitudes as demonstrated in Fig. 5(b). This lack of
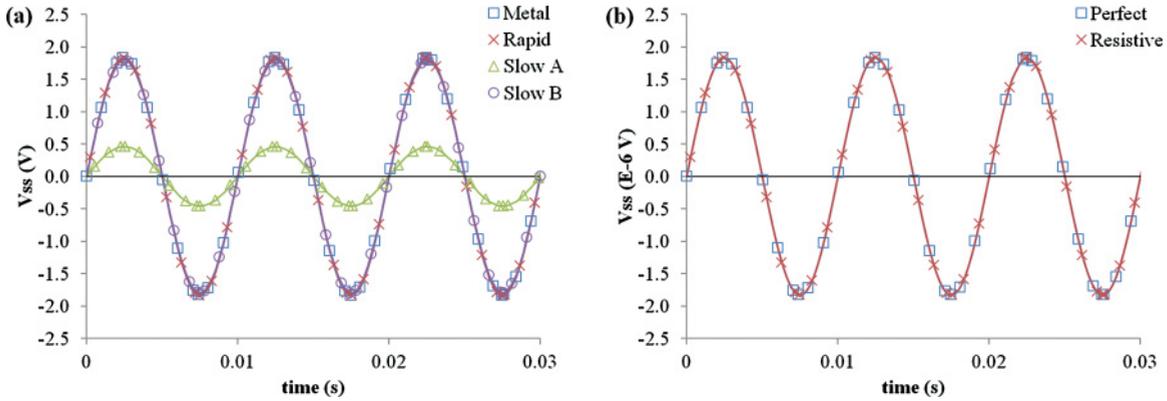
FIG. 5. (Color online) (a) V_{ss} solution for theoretical cases: metal, conductive dielectric with rapid relaxation, conductive dielectric with slow relaxation: A: $\varepsilon_2 = (1000)(\varepsilon_0)$ and B: $\varepsilon_2 = (100\,000)(\varepsilon_0)$. (b) V_{ss} solution for theoretical cases: perfect dielectric and resistive bulk.

difference can be attributed to the remarkably low amounts of currents utilized in the Kelvin probe system. For the metal case, for example, the current magnitude is approximately 1×10^{-11} A, whereas the amplitude for the perfect dielectric case is as low as 1×10^{-17} A.

These sinusoidal V_r graphs in Fig. 5 reveal no evident phase shift. As listed in Table I, the calculated phase shift between the tip-oscillation and V_r for all cases, except for the bulk resistive condition, is given by the relationship

$$\theta = \tan^{-1}(-R_{\text{in}} C_p \omega). \qquad (4.3)$$

Accordingly, to obtain a phase shift as small as $1°$, the following condition must hold: $R_{\text{in}} C_p > 2E - 3$. However, the input resistance for the Kelvin probe I-V converter is small: ~ 20 Ω, and the parasitic capacitance is similarly minute: 100 pF, making any phase shift unlikely in these cases. Even with the bulk resistive example, the phase shift is on the order of 10^{-6} radians across a large range of bulk resistance values. One situation where phase shifts may become visibly evident is when there is an actual temporal lag in the specimen's charge relaxation with respect to the tip (and thus electrical field) oscillations. Although this particular condition was not evaluated in this study [we assumed either rapid ($\tau \ll t_1$) or slow ($\tau \gg t_1$) relaxations], these results assure future Kelvin

probe users that any meaningful phase shifts are attributed to actual temporal processes within the specimen's surface and not to the circuit or to the resistive components within the bulk.

Figure 6 shows the V_{ptp} versus V_b plots for the six hypothetical cases. As demonstrated in Fig. 6(a), the metal, rapid relaxation, and slow relaxation B conditions have identical linear relationships, whereas slow relaxation A is associated with a reduced slope. Despite the identical tip-to-specimen distances across the four cases, the slopes differ and indicate that GD—as measured by the Kelvin probe—will not be an accurate marker of tip-to-specimen distance. Similarly, the perfect dielectric and resistive bulk conditions are associated with a much reduced GD as seen in Fig. 6(b) (the y axis is rescaled by six orders of magnitude for presentation purposes). As explained previously, these differences are attributed to the dielectric coefficient Eq. (4.2) and imply that GD can be greatly influenced by ε_2 and d_2. For future studies of dielectric materials, these factors should be considered if GD is to be employed as a marker of tip-to-specimen distance.

However, if GD is indeed a function of ε_2 and d_2 then theoretically GD may be utilized to provide further insights into these properties. To further extract this information, the tip-to-specimen distance (d_0) may be adjusted at predefined step intervals as the GD is recorded, and the data subsequently
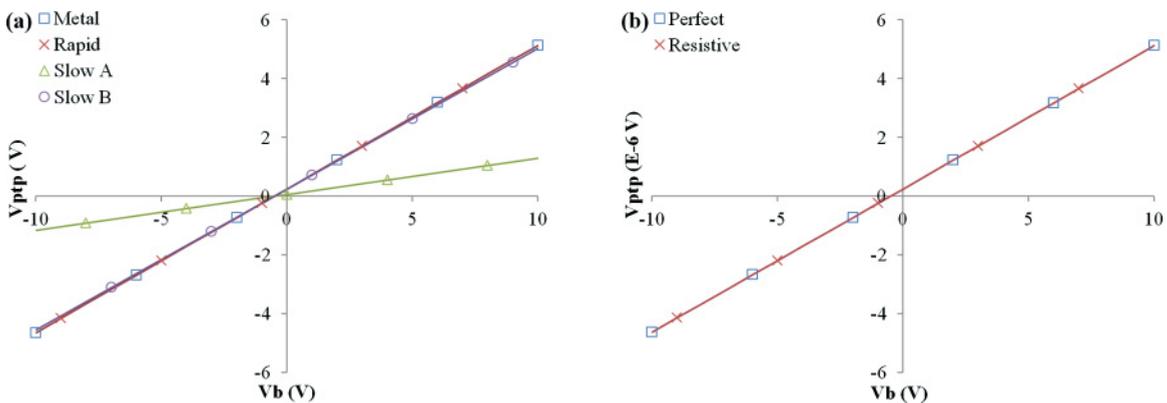

FIG. 6. (Color online) (a) V_{ptp} versus V_b plot for theoretical cases: metal, conductive dielectric with rapid relaxation, conductive dielectric with slow relaxation: A: $\varepsilon_2 = (1000)(\varepsilon_0)$ and B: $\varepsilon_2 = (100\,000)(\varepsilon_0)$. (b) V_{ptp} versus V_b plot for theoretical cases: perfect dielectric and resistive bulk.
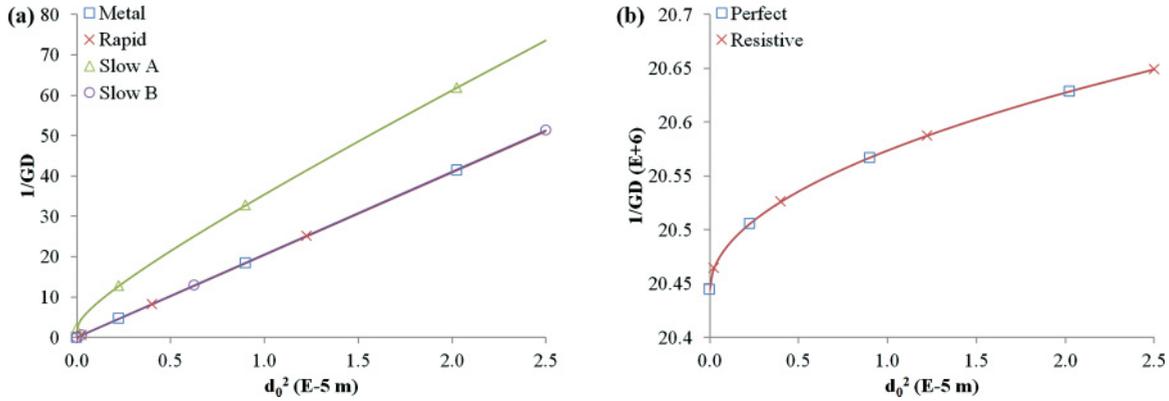
FIG. 7. (Color online) (a) $1/GD$ versus d_0^2 plot for theoretical cases: metal, conductive dielectric with rapid relaxation, conductive dielectric with slow relaxation: A: $\varepsilon_2 = (1000)(\varepsilon_0)$ and B: $\varepsilon_2 = (100\,000)(\varepsilon_0)$. (b) $1/GD$ versus d_0^2 plot for theoretical cases: perfect dielectric and resistive bulk.

utilized to produce a $1/GD$ versus d_0^2 plot. This graph is helpful because $1/GD$ is proportional to the coefficient

$$\frac{(\varepsilon_2 d_0 + \varepsilon_1 d_2)^2}{\varepsilon_1 \varepsilon_2^2}. \tag{4.4}$$

It would be directly related to d_0^2 if d_2 were negligible or if ε_2 were substantially elevated. Figure 7 reveals that metal, rapid relaxation, and slow relaxation B are all associated with a linear plot, even as the tip approaches the specimen's surface. Importantly, this linearity arises from different reasons: for metal and rapid relaxation, it arises from a negligible d_2, while for slow relaxation B, it is derived from a remarkably elevated ε_2. On the other hand, slow relaxation a generates a nonlinear plot, particularly close to the surface, and, likewise, the perfect dielectric and resistive bulk yield a nonlinear plot as demonstrated in Fig. 7(b). These curvatures arise from the fact that $\varepsilon_2 d_0$ is within the same scale as $\varepsilon_1 d_2$. Again noted in Fig. 7(b) is the negligible effect of bulk resistance on these plots.

The $1/GD$ versus d_0^2 plot can theoretically be analyzed to derive ε_2 and d_2. As illustrated in Fig. 7(b), the y intercept is a nonzero value that is proportional to d_2^2/ε_2^2, whereas the nonlinear plot is a function of the coefficient in Eq. (4.4). These two aspects of the plot can be evaluated to provide an estimate of ε_2 and d_2, assuming a known ε_1 and d_0. Moreover,

the charge relaxation rate—which is also a function of these parameters and can be assessed as V_r is measured over time—can add additional corroborative information about these important properties of the specimen. The challenge, however, is to obtain an accurate GD when d_0 is zero considering that the tip is vibrating and that the $d_0 \gg d_a$ assumption is no longer valid.

To assess the effects of d_2, Fig. 8 shows the $1/GD$ versus d_0^2 plots across a range of d_2 for both slow relaxation A and slow relaxation B conditions. As d_2 becomes smaller in magnitude, the plot is increasingly linear as shown in Fig. 8(a). Figure 8(b) provides a log-log plot of the data and reveals that, within a given case (A or B), increasing d_2 by one order of magnitude proportionally increases the y intercept value by two orders of magnitude. This is attributed to the $\varepsilon_1^2 d_2^2$ term in the coefficient. Similarly, for a given d_2, the y intercept affiliated with case A is four orders greater than case B and traced to the two orders greater magnitude ε_2. As expected, the slow relaxation A line with d_2 equal to 1 cm identically matches the slow relaxation B line with d_2 equal to 1 m, indicated by the triangle marker inside the circle marker.

C. Biomaterial cases

The biological examples in Table III B outline a variety of human biomaterials with distinct electrical properties. To
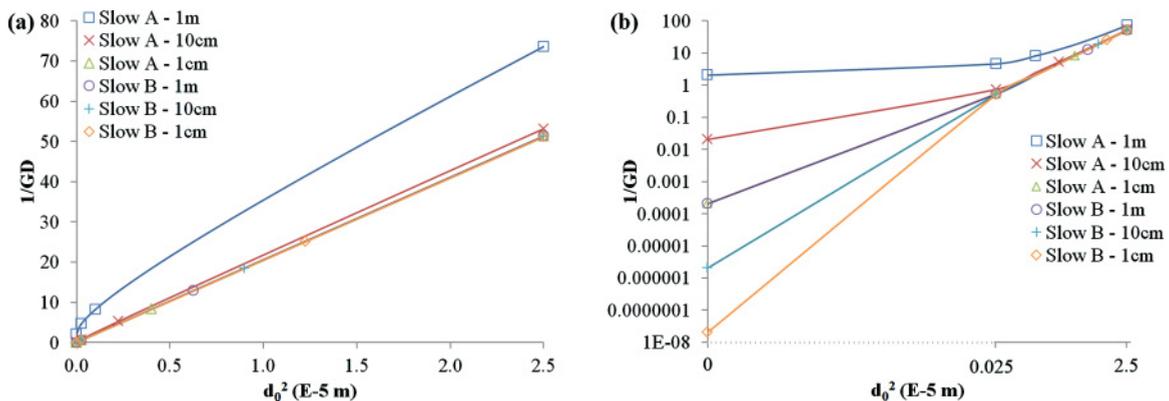

FIG. 8. (Color online) (a) $1/GD$ versus d_0^2 plot for conductive dielectric with slow relaxation: A: $\varepsilon_2 = (1000)(\varepsilon_0)$ and B: $\varepsilon_2 = (100\,000)(\varepsilon_0)$. For each case, A and B, three different values for d_2 are plotted: $d_2 = 1$ m, $d_2 = 10$ cm, and $d_2 = 1$ cm. (b) Log-log plot of $1/GD$ versus d_0^2 for the data shown in part (a) of this figure.
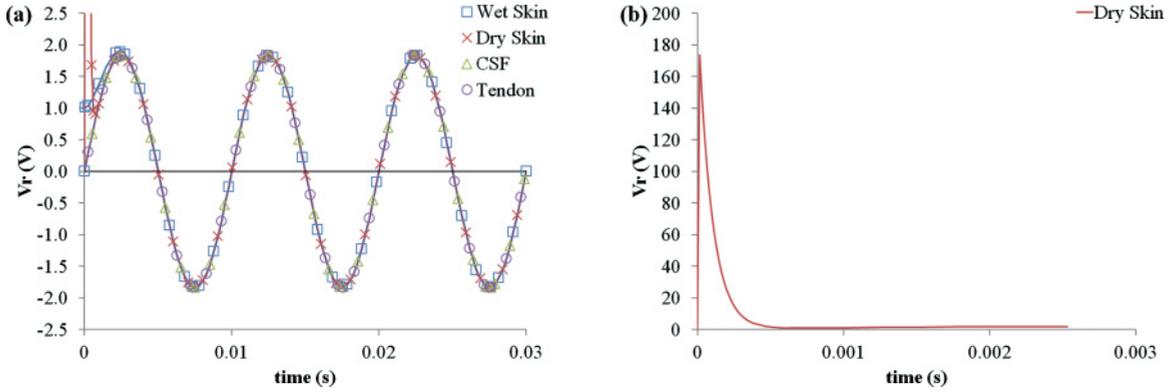
FIG. 9. (Color online) (a) V_{ss} solution for biomaterial cases: wet skin, dry skin, cerebrospinal fluid (CSF), and tendon. (b) Plot of the large, fast transient for the dry skin solution from part (a) of this figure.

analyze how these properties affect the Kelvin probe measurement, the complete solution for a conductive dielectric is used without making any assumptions regarding the relaxation rate constants when compared to the tip oscillation periods. The relaxation time for each material was calculated using Eq. (3.9), and, as seen in Table III B, the times are all less than 1 ms. Relaxation time is generally proportional to permittivity and inversely proportional to conductivity. The field penetration depths were also calculated using Eq. (4.1) and listed in Table III B. Due to the uniformly large values, a more realistic value of 1 m was used for all specimens.

Figure 9(a) displays the V_r amplitudes with respect to time for all four biomaterial cases. Wet and dry skin possesses a transient V_r component which quickly settles by the time the first wave-form peak is realized. This rapid settling ensures that the transient term has little to no effect on the peak-to-peak calculations performed by the Kelvin probe system. In Fig. 9(b), the y axis is rescaled to reveal the large, yet short-lasting transient associated with dry skin. As seen in Eq. (3.8), the transient term is proportional to the rearranged coefficient,

$$\left(\frac{\varepsilon_1 d_2}{\varepsilon_2 d_1^2 + \varepsilon_1 d_2 d_1} \right) e^{-t/\tau}. \qquad (4.5)$$

When $\varepsilon_2 d_1^2 > \varepsilon_1 d_2 d_1$ as it is in wet and dry skin, the magnitude of the transient term will be proportional to $1/\varepsilon_2$. Because dry skin has a comparatively smaller ε_2 relative to wet skin and tendon, the peak magnitude of its transient term is the largest of the three. The settling times for wet skin and tendon, however, are larger and attributed to the larger permittivity. The tendon's transient effect is not seen in Fig. 9 due its small amplitude. Although cerebrospinal fluid is associated with the smallest permittivity, the $\varepsilon_1 d_2 d_1$ term is no longer negligible and therefore yields an effectively smaller transient magnitude. These transient effects will be relevant if the capturing rate were increased or if the specimen possessed larger charge relaxation times.

For the cases considered here based on the complete solution for a conductive dielectric it is important to note that there is a dc offset term. However, this term is generally insignificant, being at least 40 orders of magnitude smaller than the oscillatory component of V_r.

Figure 10 provides plots of V_{ptp} versus V_b for the selected biomaterials, and it is evident that the four plots are identical.

Given the small relaxation times for all cases relative to the maximum V_s capture rate of the Kelvin probe system ($\sim$20 Hz), all four biomaterials are classified as rapid relaxation specimens and therefore act similarly to highly conductive materials such as metals. This conclusion is corroborated by our preliminary data of Kelvin probe measurements on human skin where, surprisingly, the V_r amplitudes were equal to those of metal. Accordingly, due to the similarity to metals, the GD measurement may also be used to accurately gauge the tip-to-specimen distance in these biomaterials.

D. Limitations

This analysis has a number of limitations. First, symbolic solutions were not obtained for the case where the tip oscillation period was within the temporal scale of the specimen relaxation time. The formulaic derivations obtained from the MAPLE symbolic software were too complex to be analyzed and incorporated within this study. Second, the Kelvin probe off-null method relies on alternating V_b (backing potential) to calculate the surface potential. These regular changes in electrical field may contribute an additional rate constant to the equations which were not fully considered within the analyses. This effect, however, is negligible if
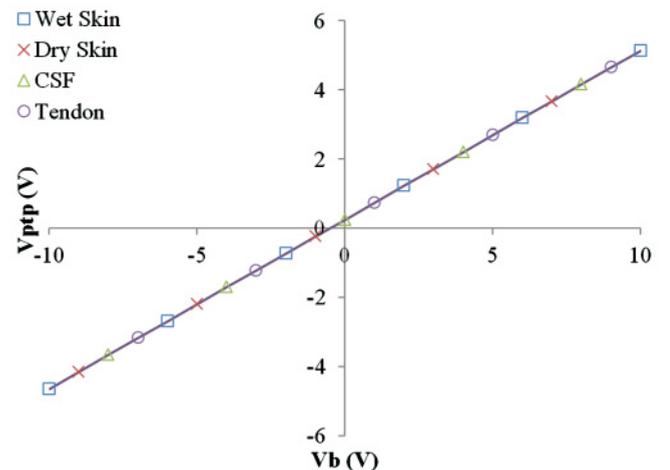

FIG. 10. (Color online) V_{ptp} versus V_b plot for biomaterial cases: wet skin, dry skin, cerebrospinal fluid (CSF), and tendon.

the specimen's charge relaxation is either much faster or much slower than the rate at which the V_b is changed. This further justifies our approach of solely focusing on the fast and slow relaxation cases. Third, we assumed a constant permittivity for all theoretical and biomaterial cases, despite the fact that permittivity, ε_2, can be complex and frequency dependent. We partially mitigated this factor by purposefully utilizing published values for permittivity and conductivity at 100 Hz. Performing our analysis in the frequency domain would have more readily incorporated complex permittivity and conductivity characteristics. We choose to keep our analysis in the time domain instead to emphasize the dynamic between the probe oscillation period and specimen settling time. Fourth, biomaterials are typically complex and composed of multiple molecular and macromolecular structures with variable permittivity and conductivity values. We simply focused on a single set of permittivity and conductivity values at a time. Fifth, these calculations are theoretical, and acquiring real-world measurements of small currents can be challenging. Obtaining accurate Kelvin probe measures may be particularly difficult in perfect dielectrics. Sixth, some biological specimen may exhibit significant surface currents in response to external low-frequency electrical fields [21]. These surface effects were not considered in our analyses. Finally, the effects of diffusion and its influence on charge relaxation and on formation of double layers were not factored in the analyses, although such processes are possible candidates for future studies.

V. CONCLUSION

For nonconductive and partially conductive materials considered in this analysis, the Kelvin probe performs in two distinct manners. If the charge relaxation in the material occurs faster than the rate of electrical field oscillations (associated with tip movement), then the Kelvin probe generates surface potential measurements and V_r amplitudes equivalent to that of highly conductive materials such as metal, and the off-null approach yields an accurate tracking measurement of the tip-to-specimen distance. If, however, the charge relaxation is much slower or occurs not at all, the Kelvin probe generates smaller V_r amplitudes and the tracking function is less accurate. Nevertheless, analyses of various Kelvin probe-generated variables may help derive the specimen's permittivity and electrical field penetration depth. The resistive components within the specimen's bulk contribute little to the overall Kelvin probe surface potential measurements.

Because of their rapid relaxation rate and increased permittivity, biomaterials behave similarly to metal when evaluated by the Kelvin probe. As a consequence, the Kelvin probe can be readily applied to measure surface potentials of biological specimens and theoretically obtain measurements with submillivolt resolution at a micrometer spatial scale without being confounded by factors attributed to electrode-specimen contact. This may have important future medical applications for evaluating electrical fields associated with wound healing, dermatological malignancies, and sweat activity.

APPENDIX A

The $V_r(t)$ solution for a perfect dielectric with a resistive bulk is provided here.

$$V_r(t) = V_{D1} + V_{D2} + V_{D3}, \tag{A1}$$

where

$$V_{D1} = (C_1)e^{-(M_x)(T_x+T_y)t}, \quad V_{D2} = (C_2)e^{-(M_x)(T_x-T_y)t}, \quad V_{D3} = \frac{V_{DN}}{V_{DD}}, \quad M_x = \frac{1}{2\varepsilon_1\varepsilon_2 R_{\text{in}} R_b C_p A}, \quad T_x = R_{\text{in}} C_p \left(\varepsilon_2 d_0 + \varepsilon_1 d_2\right),$$

$$T_y = \sqrt{R_{\text{in}}^2 C_p^2 \left(\varepsilon_2 d_0 + \varepsilon_1 d_2\right)^2 + \left(-4\varepsilon_1\varepsilon_2 R_{\text{in}} R_b C_p A\right)\left(\varepsilon_2 d_0 + \varepsilon_1 d_2\right)},$$

$$V_{DN} = R_{\text{in}}\varepsilon_1\varepsilon_2^2 d_a A\omega[(\varepsilon_1 d_2 + \varepsilon_2 d_0)(\omega R_{\text{in}} C_p \cos(\omega t) - \sin(\omega t)) - \varepsilon_1\varepsilon_2 R_{\text{in}} R_b C_p \omega^2 A \sin(\omega t)](V_b + V_s),$$

$$V_{DD} = (\varepsilon_2 d_0 + \varepsilon_1 d_2)\left[(-2\varepsilon_1\varepsilon_2 R_{\text{in}} R_b C_p A\omega^2)(\varepsilon_2 d_0 + \varepsilon_1 d_2) + (\varepsilon_2 d_0 + \varepsilon_1 d_2)^2 + \left(R_{\text{in}}^2 C_p^2 \omega^2\right)(\varepsilon_2 d_0 + \varepsilon_1 d_2)^2 + \varepsilon_1^2\varepsilon_2^2 R_{\text{in}}^2 R_b^2 C_P^2 A^2 \omega^2\right].$$

[1] I. D. Baikie, P. J. S. Smith, D. M. Porterfield, and P. J. Estrup, Rev. Sci. Instrum. **70**, 1842 (1999).

[2] H. N. McMurray, A. J. Coleman, G. Williams, A. Afseth, and G. M. Scamans, J. Electrochem. Soc. **154**, C339 (2007).

[3] G. S. Frankel, M. Stratmann, M. Rohwerder, A. Michalik, B. Maier, J. Dora, and M. Wicinski, Corros. Sci. **49**, 2021 (2007).

[4] D. M. Taylor and G. F. Bayes, Mater. Sci. Eng., C **8–9**, 65 (1999).

[5] D. M. Taylor, Adv. Colloid Interface Sci. **87**, 183 (2000).

[6] D. A. Gorin, A. M. Yashchenok, A. O. Manturov, T. A. Kolesnikova, and H. Mohwald, Langmuir **25**, 12529 (2009).

[7] I. Lange, J. C. Blakesley, J. Frisch, A. Vollmer, N. Koch, and D. Neher, Phys. Rev. Lett. **106**, 216402 (2011).

[8] S. E. Park, N. V. Nguyen, J. J. Kopanski, J. S. Suehle, and E. M. Vogel, J. Vac. Sci. Technol. B **24**, 404 (2006).

[9] G. Williams, A. Gabriel, A. Cook, and H. N. McMurray, J. Electrochem. Soc. **153**, B425 (2006).

[10] B. S. Simpkins, E. T. Yu, U. Chowdhury, M. M. Wong, T. G. Zhu, D. W. Yoo, and R. D. Dupuis, J. Appl. Phys. **95**, 6225 (2004).

[11] C. S. Jiang, H. R. Moutinho, D. J. Friedman, J. F. Geisz, and M. M. Al-Jassim, J. Appl. Phys. **93**, 10035 (2003).

[12] O. A. Semenikhin, L. Jiang, K. Hashimoto, and A. Fujishima, Synth. Met. **110**, 115 (2000).

[13] I. D. Baikie, S. Mackenzie, P. J. Z. Estrup, and J. A. Meyer, Rev. Sci. Instrum. **62**, 1326 (1991).

[14] I. D. Baikie, E. Venderbosch, J. A. Meyer, and P. J. Z. Estrup, Rev. Sci. Instrum. **62**, 725 (1991).

[15] I. D. Baikie and P. J. Estrup, Rev. Sci. Instrum. **69**, 3902 (1998).

[16] R. Nuccitelli, P. Nuccitelli, S. Ramlatchan, R. Sanger, and P. J. Smith, Wound Repair and Regeneration **16**, 432 (2008).

[17] A. Grodzinsky, *Fields, Forces and Flows in Biological Systems* (Garland Science, New York, 2011).

[18] S. Grimnes and O. G. Martinsen, *Bioimpedance and Bioelectricity Basics* (Academic Press, Oxford, 2008).

[19] S. Gabriel, R. W. Lau, and C. Gabriel, Phys. Med. Biol. **41**, 2271 (1996).

[20] C. Gabriel, in *Compilation of the dielectric properties of body tissues at RF and microwave frequencies*, Report AL/OE-TR-1996-0037 (Occupational and Environmental Health Directorate, Radiofrequency Radiation Division, Brooks Air Force Base, TX, 1996).

[21] E. Prodan, C. Prodan, and J. H. Miller Jr., Biophys. J. **95**, 4174 (2008).